A real-time fast radio burst: polarization detection and multiwavelength follow-up

E. Petroff, M. Bailes, E. D. Barr, B. R. Barsdell, N. D. R. Bhat, F. Bian, S. Burke-Spolaor, M. Caleb, D. Champion, P. Chandra, et al.

Monthly Notices
of the
ROYAL ASTRONOMICAL SOCIETY

MNRAS **447,** 246–255 (2015) doi:10.1093/mnras/stu2419

A real-time fast radio burst: polarization detection and multiwavelength follow-up

E. Petroff,[1,2,3★] M. Bailes,[1,3] E. D. Barr,[1,3] B. R. Barsdell,[4] N. D. R. Bhat,[3,5] F. Bian,[6†] S. Burke-Spolaor,[7] M. Caleb,[1,3,6] D. Champion,[8] P. Chandra,[9] G. Da Costa,[6] C. Delvaux,[10] C. Flynn,[1,3] N. Gehrels,[11] J. Greiner,[10] A. Jameson,[1,3] S. Johnston,[2] M. M. Kasliwal,[12‡] E. F. Keane,[1,3] S. Keller,[6] J. Kocz,[4,13] M. Kramer,[8,14] G. Leloudas,[15,16] D. Malesani,[15] J. S. Mulchaey,[12] C. Ng,[8] E. O. Ofek,[16] D. A. Perley,[7‡] A. Possenti,[17] B. P. Schmidt,[3,6] Yue Shen,[13,18] B. Stappers,[14] P. Tisserand,[3,6,19,20] W. van Straten[1,3] and C. Wolf[3,6]

Affiliations are listed at the end of the paper

Accepted 2014 November 12. Received 2014 November 11; in original form 2014 September 14

ABSTRACT

Fast radio bursts (FRBs) are one of the most tantalizing mysteries of the radio sky; their progenitors and origins remain unknown and until now no rapid multiwavelength follow-up of an FRB has been possible. New instrumentation has decreased the time between observation and discovery from years to seconds, and enables polarimetry to be performed on FRBs for the first time. We have discovered an FRB (FRB 140514) in real-time on 2014 May 14 at 17:14:11.06 UTC at the Parkes radio telescope and triggered follow-up at other wavelengths within hours of the event. FRB 140514 was found with a dispersion measure (DM) of 562.7(6) cm^{-3} pc, giving an upper limit on source redshift of $z \lesssim 0.5$. FRB 140514 was found to be 21 ± 7 per cent (3σ) circularly polarized on the leading edge with a 1σ upper limit on linear polarization <10 per cent. We conclude that this polarization is intrinsic to the FRB. If there was any intrinsic linear polarization, as might be expected from coherent emission, then it may have been depolarized by Faraday rotation caused by passing through strong magnetic fields and/or high-density environments. FRB 140514 was discovered during a campaign to re-observe known FRB fields, and lies close to a previous discovery, FRB 110220; based on the difference in DMs of these bursts and time-on-sky arguments, we attribute the proximity to sampling bias and conclude that they are distinct objects. Follow-up conducted by 12 telescopes observing from X-ray to radio wavelengths was unable to identify a variable multiwavelength counterpart, allowing us to rule out models in which FRBs originate from nearby ($z < 0.3$) supernovae and long duration gamma-ray bursts.

Key words: polarization – radiation mechanisms: general – intergalactic medium – radio continuum: general.

1 INTRODUCTION

A new class of objects called fast radio bursts (FRBs) have been discovered in radio pulsar surveys at Parkes and Arecibo within the last decade (Lorimer et al. 2007; Thornton et al. 2013; Burke-Spolaor & Bannister 2014; Spitler et al. 2014). All FRBs discovered to date have been single radio events of millisecond duration. The electron column density, called the dispersion measure (DM), is also uncharacteristically high, leading to theories that they originate at cosmological distances (Thornton et al. 2013) and/or in extreme environments (Katz 2014; Lyubarsky 2014). Recently, they have been the topic of considerable discussion, both as to their origins and their potential use as cosmological tools (Deng & Zhang 2014; Gao, Li & Zhang 2014; Kulkarni et al. 2014; Loeb, Shvartzvald & Maoz 2014).

★ E-mail: epetroff@astro.swin.edu.au
† Stromlo Fellow.
‡ Hubble Fellow.

Thornton et al. (2013) measure a rate of $R_{\rm FRB}(\mathcal{F} \sim 3$ Jy ms) $\sim 1.0^{+0.6}_{-0.5} \times 10^4$ sky^{-1} d^{-1} from four events found in a high Galactic latitude search, but the non-detection of FRBs in a survey twice as long suggests either a lower overall FRB rate or a latitude dependence, owing to a currently unknown obscuration effect at Galactic latitudes below $|b| = 15^\circ$ (Petroff et al. 2014). This result has recently been confirmed by Burke-Spolaor & Bannister (2014). The true progenitors of FRBs remain unknown. All published FRBs were discovered in archival data years later and rapid follow-up of an FRB has never been possible.

Recent efforts in time-domain radio astronomy have focused on real-time FRB detection with the promise of rapid follow-up of new events. Such capability was recently made possible with the development of a real-time transient pipeline at the Parkes telescope. A new survey at Parkes aims to search the fields of previous FRB events for repeating bursts, a direct prediction made by flare star and magnetar flare origin theories (Kulkarni et al. 2014; Loeb et al. 2014). The discovery of repeating FRB sources would strongly constrain emission mechanisms and possible progenitors.

Here, we report on early results from this survey with the discovery of a new FRB in the field of FRB 110220. In Section 2, we describe the real-time transient pipeline at Parkes using the multibeam receiver. In Section 3, we present the detection of FRB 140514 and, for the first time, the polarized radiation of an FRB. Section 4 details the follow-up efforts from X-ray to radio from 12 observatories. We summarize the results from these follow-ups in Section 5 and discuss polarization in Section 5.1, connections between FRB 140514 and FRB 110220 in Section 5.2, and limits on an afterglow in Section 5.3. We provide a conclusion in Section 6.

2 REAL-TIME TRANSIENT PIPELINE

Observations were conducted with the Berkeley Parkes Swinburne Recorder (BPSR) backend for the 13-beam multibeam receiver (Staveley-Smith et al. 1996) at Parkes which covers 0.5 deg^2 on the sky. We record 8-bit full-polarization data from two orthogonal linear feeds per beam, with 1024 frequency channels over 400 MHz of bandwidth, from 1182to1582 MHz, and 64-μs time resolution. Data are passed to the HI-Pulsar Signal Processor where 120 s of observations are stored in a ring buffer using PSRDada.[1] The effective bandwidth for our data is 340 MHz from 1182to1522 MHz due to communications satellites operating in the 1525–1559 MHz band (Keith et al. 2010). The observing instrumentation is identical to that used for the High Time Resolution Universe survey and the FRB discoveries reported in Thornton et al. (2013).

The real-time processing of the data for transient events is performed on the buffer using the HEIMDALL single pulse processing software.[2] The linear polarizations are summed into a single 8-bit data set and are passed to HEIMDALL in 256 kilosample chunks (approximately 16.77 s). If a candidate is detected, the relevant 8-bit data are saved to disk. HEIMDALL performs a search for pulses across a specified range of DMs and pulse widths and returns a list of candidates. The real-time transient pipeline searches 0–2000 cm^{-3} pc in DM and 0.128–262 ms in pulse width and identifies candidates that fit a number of criteria attributable to known FRBs:

$$\begin{aligned}
&{\rm DM} \geq 1.5 \times {\rm DM_{MW}} \\
&{\rm S/N} \geq 10 \\
&N_{\rm beams} \leq 4 \\
&\Delta t \leq 8.192 \text{ ms} \\
&N_{\rm events}(t_{\rm obs} - 2\text{ s} \rightarrow t_{\rm obs} + 2\text{ s}) \leq 5,
\end{aligned} \tag{1}$$

where $\rm DM_{MW}$ is the Galactic DM along the line of sight predicted by the NE2001 electron density model (Cordes & Lazio 2002), S/N is the signal to noise ratio, $N_{\rm beams}$ is the number of beams in which the candidate appears, Δt is the pulse width, and $N_{\rm events}(t_{\rm obs} - 2\,{\rm s} \rightarrow t_{\rm obs} + 2\,{\rm s})$ is the number of separately identified pulse candidates within a 4 s window around the candidate, more than the expected time duration of a single burst with DM ≤ 2000 pc cm^{-3}. For each candidate which meets all criteria above, we also check that there is no known pulsar in the pulsar catalogue (Manchester et al. 2005) within a 5 per cent DM range of the candidate for completeness, although this condition is typically precluded by the high-DM threshold. All known archival FRBs are identified using these criteria.

When a candidate is detected the observable time span of the event is calculated using the total DM delay, $\tau_{\rm DM}$, across our observing bandwidth:

$$\tau_{\rm DM} = 4.15\ {\rm DM} \left(\nu_{\rm low}^{-2} - \nu_{\rm high}^{-2}\right)\ \text{ms}, \tag{2}$$

where $\nu_{\rm low}$ and $\nu_{\rm high}$ are the lowest and highest frequencies in the band, in GHz, and DM is in pc cm^{-3}. For all BPSR data $\nu_{\rm low} = 1.182$ GHz and $\nu_{\rm high} = 1.582$ GHz. The start time of the event is identified in the 120 s buffer and all samples in the range $(t_{\rm start} - \tau_{\rm DM}, t_{\rm start} + 2\tau_{\rm DM})$ are saved to disk with full polarization 8-bit data.

The BPSR real-time candidate detection and polarization triggering mode was commissioned in 2014 March. Previously, it was impossible to obtain polarization data for FRBs at Parkes. Currently, the triggers are configured to give a few false positives rather than miss a real event, and the real-time nature of the pipeline enables the trained observer to provide immediate feedback. The triggers have not yet been connected directly with other telescopes, but instead only initiate an email alert to observers related to the project when an event satisfying the above criteria is found.

3 PARKES REAL-TIME DETECTION OF FRB 140514

FRB 140514 was discovered on 2014 May 14 at 17:14:11.06 UTC (May 15 03:14:11.06 local time) at 1.4 GHz in the centre beam (beam 01) of the multibeam receiver. It was identified in the HEIMDALL real-time transient pipeline with an S/N of 16, a DM of 562.7(6) pc cm^{-3}, and a pulse width of $2.8^{+3.5}_{-0.7}$ ms. The pipeline identified the burst within 10 s, and 2.22 s of data around the event were recorded to disk in 8-bit dual polarization for all 13 beams of the receiver. An FRB alert email was sent to project observers at 17:14:30 UTC.

If the burst occurred at the beam-centre the detection corresponds to a peak flux density of $0.47\ ^{+0.11}_{-0.08}$ Jy and a fluence of $1.3\ ^{+2.3}_{-0.5}$ Jy ms. Further analysis of the FRB data resulted in a dispersion index $\alpha = -2.000(4)$ such that $\delta t \propto {\rm DM}\,\nu^\alpha$, in agreement with the ν^{-2} expected for cold plasma. The scattering time-scale was found to be $\tau_{1\,\rm GHz} = 5.4(1)$ ms. There is a decreased uncertainty in the dispersion index and the scattering time-scale, as the scattering index was not a free parameter in the fit algorithm. While the scattering modelling done for these fits is consistent with a range of different pulse widths,

[1] http://psrdada.sourceforge.net
[2] http://sourceforge.net/projects/heimdall-astro/

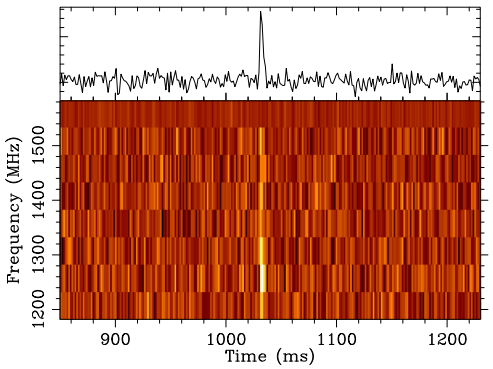

Figure 1. The pulse profile and dynamic spectrum of FRB 140514 with pulse width $2.8^{+3.5}_{-0.7}$ ms, dedispersed to DM = 562.7 pc cm^{-3} and summed to eight frequency channels across the band. The total time plotted has been reduced to 400 ms for greater clarity. Frequency channels between 1520 and 1580 MHz are excised due to narrow-band radio interference from the Thuraya 3 satellite which transmits in this band.

leading to large error in Δt, the effect on the scattering tail, and thus $\tau_{1\,\mathrm{GHz}}$, is negligible, giving a smaller error.

The DM, dispersion index and scattering time-scale were all fit for while the scattering index was held fixed at $\beta = -4$. The limited S/N (16) of the pulse prohibited fitting for β due to strong covariances between the four quantities. See Fig. 1 and Table 1 for all observed FRB parameters, and Table 2 for derived cosmological parameters.

All 13 beams of full-Stokes data were analysed in detail and the pulse was not detected in any other beam of the receiver. Since there was no coincident detection in other beams, we conclude that the event was not a sidelobe detection. Therefore, we have used the coordinates from the beam centre for the detection pointing with an error diameter of 14.4 arcmin, the approximate full width half-maximum (FWHM) of beam 01 at 1.4 GHz (Staveley-Smith et al. 1996).

Table 1. Observed properties of FRB 140514.

Event date UTC	14 May 2014
Event time UTC, $\nu_{1.4\,\mathrm{GHz}}$	17:14:11.06
Event time, ν_∞	17:14:09.83
Local date AEST	15 May 2014
Local time AEST	03:14:11.06
RA	22:34:06.2
Dec.	−12:18:46.5
(ℓ, b)	(50.°8, −54.°6)
Beam diameter	14.4 arcmin
$\mathrm{DM_{FRB}}$ (pc cm^{-3})	562.7(6)
$\mathrm{DM_{MW}}$ (pc cm^{-3})	34.9
Detection S/N	16(1)
Observed width, Δt (ms)	$2.8^{+3.5}_{-0.7}$
Scattering time-scale, $\tau_{1\,\mathrm{GHz}}$ (ms)	5.4(1)
Dispersion index, α	−2.000(4)
Peak flux density, $S_{\nu,\,1400\,\mathrm{MHz}}$ (Jy)	$0.47^{+0.11}_{-0.08}$
Fluence, $\mathcal{F}$ (Jy ms)	$1.3^{+2.3}_{-0.5}$

Table 2. Derived cosmological properties of FRB 140514.

z	$< 0.44(1)$
Comoving distance (Gpc)	$< 1.71(3)$
Luminosity distance (Gpc)	$< 2.46^{+0.04}_{-0.06}$
Energy (erg)	$< 3.7^{+4.7}_{-2.0} \times 10^{38}$
Distance modulus (mag)	< 42.2

FRB 140514 was discovered in a pointing centred just 9 arcmin away from the nominal position of known FRB 110220 during a standard gridding (Morris et al. 2002) of the region in our survey. The previous event nearby, FRB 110220, had DM = 944.38(5) pc cm^{-3} and a peak flux density of 1.3 Jy, if it occurred at beam-centre.

Models of the free electron content of the Milky Way predict that the ionized Galactic interstellar medium contribution to the DM of FRB 140514 is only 35 pc cm^{-3} (Cordes & Lazio 2002), only 6 per cent of the total, which sets an upper limit on redshift $z < 0.4(1)$ based on ionization models of the intergalactic medium (IGM), making no assumptions about a host contribution to the total DM, and assuming an upper limit on the Galactic DM contribution of 70 pc cm^{-3} (Ioka 2003). This upper limit on redshift corresponds to a comoving distance of $<1.71(3)$ Gpc, a luminosity distance of $<2.46^{+0.04}_{-0.06}$ Gpc, an energy of $<3.7^{+4.7}_{-2.0} \times 10^{38}$ erg, and a distance modulus of <42.2 mag (Wright 2006). In comparison, the upper limit on redshift for FRB 110220 was $z < 0.81$, which corresponds to a comoving distance of 2.8 Gpc, a luminosity distance of 5.1 Gpc, and a distance modulus of 43.5 mag (Thornton et al. 2013) if most of the excess DM is attributed to the IGM.

A calibration observation was taken at the end of the observing session at 01:04:39 UTC on May 15, 7 h 50 m after FRB 140514, which was used to calibrate the polarized data. The feed was assumed to be ideal and the calibration was performed using the `pac` command in the PSRCHIVE software package[3] (Hotan, van Straten & Manchester 2004). We did not perform a Mueller matrix calculation as we cannot determine the exact location of the FRB within the Parkes beam. From the calibration of the orthogonal linear feeds, we obtained all four Stokes parameters, plotted in Fig. 2; this represents the first detection of polarized flux from an FRB.

The emission of FRB 140514 was polarized with 21 ± 7 per cent (3σ) circular polarization averaged over the whole pulse. On the leading edge of the pulse, however, the pulse is 42 ± 9 per cent circularly polarized, a 5σ detection. No linear polarization was detected and we place a 1σ upper limit of 10 per cent of the total intensity (Fig. 2). We note that it would require a very rare and specific feed rotation to result in high fractional circular polarization with no linear detection. Such a configuration would also result in a high correlation between Stokes V and I, and we do not observe the circular polarization to tightly follow the total intensity. The measured circular polarization is determined to be intrinsic to the observation, and not a calibration artefact.

With a polarized signal it is possible to measure the Faraday rotation of the Stokes vectors as a function of frequency due to the magnetic field and electron column density along the line of sight. The amount of induced rotation is quantified by the rotation measure,

$$\mathrm{RM} \propto \int_0^d n_\mathrm{e} B_\parallel \mathrm{d}l \,, \tag{3}$$

where d is the distance to the source, n_e is the electron column density, and $B_\parallel$ is the magnetic field parallel to the line of sight such that the rotation angle of the linear polarization $\Delta\Psi = \mathrm{RM}\lambda^2$ (Lorimer & Kramer 2004). An optimal rotation measure search was performed using the RMFIT code in the PSRCHIVE pulsar

[3] http://psrchive.sourceforge.net/index.shtml

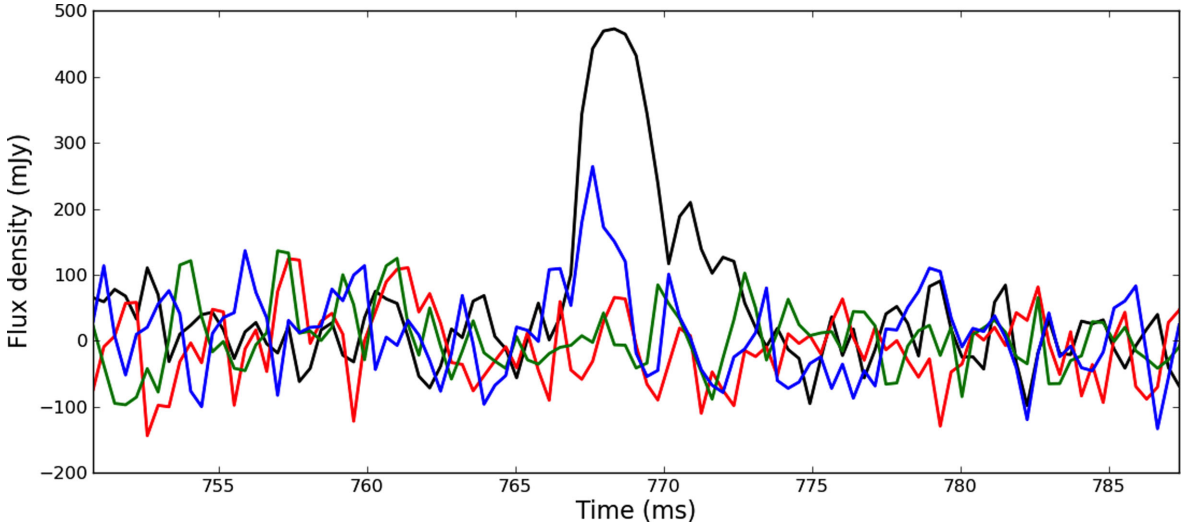

Figure 2. The full-Stokes parameters of FRB 140514 recorded in the centre beam of the multibeam receiver with BPSR. Total intensity, and Stokes Q, U, and V are represented in black, red, green, and blue, respectively. FRB 140514 has 21 ± 7 per cent (3σ) circular polarization averaged over the pulse, and a 1σ upper limit on linear polarization of $L < 10$ per cent. On the leading edge of the pulse the circular polarization is 42 ± 9 per cent (5σ) of the total intensity. The data have been smoothed from an initial sampling of 64 μs using a Gaussian filter of FWHM 90 μs.

software package out to $|\mathrm{RM_{max}}| = 1.18 \times 10^5$ rad m^{-2}, the rotation measure (RM) at which the signal is completely depolarized within a single frequency channel at our observing frequency. No linear polarization was evident at $\geq 3\sigma$ significance.

4 FRB FOLLOW-UP AT OTHER TELESCOPES

The real-time detection of FRB 140514 enabled an extensive coordination of telescopes and multiwavelength observations. Three sources of interest were identified in the 14.4 arcmin diameter of the Parkes beam: two X-ray sources detected by *Swift*, referred to below as XRT1 and XRT2, and one from the Giant Metrewave Radio Telescope (GMRT), referred to as GMRT1. The search for a counterpart focused on identification of any variable slow transients in the field that either brightened or dimmed by >2 mag between epochs. For objects near the magnitude limit of the observation (the magnitude of the dimmest detectable source in the observation), an appearance or disappearance between epochs was only considered significant if the source was 2 mag or more above the limit in one observing epoch. Ultimately, no afterglow-like counterpart was identified at any wavelength involved in this effort. Here, we report on the findings from 12 telescopes involved in the follow-up effort, listed in Table 3.

4.1 Parkes Radio Telescope

FRB 140514 was discovered in the first grid pointing around the position of FRB 110220 of the observing session, 9 arcmin away from the previous FRB discovery position, less than one beamwidth (Thornton et al. 2013). A grid of the field was observed for another 1.6 h after detection as part of the scheduled observations, and then again at the end of the observing session, 7 h after discovery, both with 145 mJy rms at 1.4 GHz. No further dispersed pulses at DM $\geq$ 5 pc cm^{-3} were detected in subsequent observations. No other FRB-like pulses were found throughout the observing session

Table 3. Follow-up observations conducted at 12 telescopes. Limits presented are the minimum detectable magnitude or flux of each epoch. All dates are for the year 2014.

Telescope	Date start time UTC	T+	Limits
Parkes	May 14 17:14:12	1 s	1.4 GHz–145 mJy
ATCA	May 15 00:10:00	7 h	5.5 GHz–40 mJy
			2 GHz–60 mJy
Parkes	May 15 23:57:38	6 h 52 m	1.4 GHz–145 mJy
Swift	May 15 01:44:43	8 h 30 m	8.2×10^{-15} erg cm^{-2} s^{-1}
GROND	May 15 08:49:30	16 h	$J - 21.1$, $H - 20.4$,
			$K - 18.4$
Swope	May 15 09:57:13	16 h 51 m	$R - 16$
iPTF	May 15 11:16:03	18 h 11 m	$R - 19.1$
Swift	May 15 16:08:44	23 h 18 m	3.9×10^{-15} erg cm^{-2} s^{-1}
GMRT	May 16 01:30:00	1.3 d	610 MHz–125 μJy
Effelsberg	May 16 06:50:00	1.4 d	4.8 GHz–2.5 mJy
iPTF	May 16 11:18:21	1.7 d	$R - 19.3$
SkyMapper	May 16 17:57:24	2 d	Hα – 17
NOT	May 17 04:48:46	2.4 d	370–730 nm
GROND	May 17 09:04:13	2.6 d	$J - 21.1$, $H - 20.5$,
			$K - 18.6$
Swope	May 17 09:50:00	2.6 d	$R - 16$
Magellan	May 17 10:11:19	2.6 d	$R - 22.5$, $I - 22.5$
iPTF	May 17 11:15:33	2.7 d	$R - 19.3$
Effelsberg	May 18 03:50:00	3.4 d	2.7 GHz–1.2 mJy
iPTF	May 19 11:23:52	4.7 d	$R - 19.1$
Effelsberg	May 21 05:35:00	7.5 d	1.4 GHz–1.2 mJy
SkyMapper	May 23 17:45:48	9 d	Hα – 17
Keck	May 27 14:06:22	12.8 d	30–1000 nm
Swift	June 02 00:06:02	18.3 d	6.35×10^{-15} erg cm^{-2} s^{-1}
GMRT	June 03 00:20:00	19.3 d	1390 MHz–61 μJy
NOT	June 05 03:51:09	21.4 d	370–730 nm
GMRT	June 08 20:30:00	24.1 d	610 MHz–150 μJy
Parkes	June 24 14:36:40	41 d	1.4 GHz–145 mJy
Magellan	July 8 07:34:44	55 d	$R - 24.5$, $I - 24.5$
Parkes	July 27 12:14:00	74 d	145 mJy

along any other sightlines, and there was no strong radio frequency interference. The field was re-observed for eight consecutive hours on June 24, 41 d after the FRB event and again for 3.5 h on July 27, 74 d after FRB 140514, and no new candidates were identified.

4.2 Australia Telescope Compact Array

The Australia Telescope Compact Array (ATCA) observed the FRB field as a target of opportunity (ToO, proposal CX293) starting at 00:10 UT on 2014 May 15, less than 7 h after the FRB. The total observing time was 3 h including calibration and overheads. Observations were made simultaneously from 4.5 to 6.5 GHz and 8 to 10 GHz for a total of 60 min on source and from 1.1 to 3.1 GHz with 60 min on source. The rms of the images are approx 40 μJy at the higher frequencies and 60 μJy at 2 GHz. GMRT1 was identified in the ATCA image with a flux density of 1.5 mJy and XRT1 was also visible with a flux density of 3 mJy. While the ATCA was the first telescope other than Parkes to image the field, the lack of a second epoch days or weeks later hampered our ability to detect variable sources at these radio frequencies. No radio source could be targeted based on the ATCA observations.

4.3 Giant Metrewave Radio Telescope

The GMRT began observing the FRB field as a ToO (proposal DDT B124) 2 d after the event at 610 MHz at 01:30 UT on May 16. The 3-h observation (including overheads and calibrators) produced an image of the field with 123 μJy rms. We identified three sources within the field of view (J2000 coordinates): GMRT1 (RA = 22:34:08.493, Dec. = −12:18:27.00), GMRT2 (RA = 22:34:19.003, Dec. = −12:21:30.38), and GMRT3 (RA = 22:34:00.088, Dec. = −12:14:50.00). The first, GMRT1, did not appear to correspond to any sources in the NRAO VLA Sky Survey catalog (NVSS; Condon et al. 1998), and was flagged for further follow-up by other telescopes as a potentially variable source given the temporal proximity of the GMRT observation and the FRB detection. The other two sources, GMRT2 and GMRT3, correlated well with positions for known radio sources in the NVSS catalog with consistent flux densities. Subsequent observations were taken through the GMRT ToO queue on May 20, June 3, and June 8 in the 325 MHz, 1390 MHz, and 610 MHz bands, respectively. The second epoch was largely unusable due to technical difficulties. The search for variability focused on monitoring each source for flux variations across observing epochs. All sources from the first epoch appeared in the third and fourth epochs with no measurable change in flux densities.

4.4 *Swift* X-ray Telescope

The first observation of the FRB 140514 field was taken using *Swift* XRT (Gehrels et al. 2004) only 8.5 h after the FRB was discovered at Parkes. This was the fastest *Swift* follow-up ever undertaken for an FRB. 4 ks of XRT data were taken in the first epoch, and a further 2 ks of data were taken in a second epoch later that day, 23 h after FRB 140514, to search for short term variability. A final epoch, 18 d later, was taken to search for long term variability. Two X-ray sources were identified in the first epoch of data within the 15 arcmin diameter of the Parkes beam. Both sources were consistent with sources in the USNO catalog (Monet et al. 2003). The first source (XRT1) is located at RA = 22:34:41.49, Dec. = −12:21:39.8 with $R_{\rm USNO}$ = 17.5 and the second (XRT2) is located at RA = 22:34:02.33 Dec. = −12:08:48.2 with $R_{\rm USNO}$ = 19.7. Both XRT1 and XRT2 appeared in all subsequent epochs with no observable variability on the level of 10 and 20 per cent for XRT1 and XRT2, respectively, both calculated from photon counts from the XRT. Both sources were later found to be active galactic nuclei (AGN).

4.5 Gamma-Ray Burst Optical/Near-Infrared Detector

After 13 h, a trigger was sent to the Gamma-Ray Burst Optical/Near-Infrared Detector (GROND) operating on the 2.2-m MPI/ESO telescope on La Silla in Chile (Greiner et al. 2008). GROND is able to observe simultaneously in *J*, *H*, and *K* near-infrared (NIR) bands with a 10 arcmin × 10 arcmin field of view (FOV) and the optical g', r', i', and z' bands with a 6arcmin × 6 arcmin FOV. A 2 × 2 tiling observation was done, providing 61 per cent (*JHK*) and 22 per cent ($g'r'i'z'$) coverage of the inner part of the FRB error circle. The first epoch began 16 h after FRB 140514 with 460 s exposures, and a second epoch was taken 2.5 d after the FRB with an identical observing setup and 690 s ($g'r'i'z'$) and 720 s (*JHK*) exposures, respectively. Limiting magnitudes for *J*, *H*, and *K* bands were 21.1, 20.4, and 18.4 in the first epoch and 21.1, 20.5, and 18.6 in the second epoch, respectively (all in the AB system). Of all the objects in the field, analysis identified three variable objects, all very close to the limiting magnitude and varying on scales of 0.2–0.8 mag in the NIR bands identified with difference imaging. Of the three objects one is a galaxy, another is likely to be an AGN, and the last is a main-sequence star. Both XRT1 and GMRT1 sources were also detected in the GROND infrared imaging but were not observed to vary in the infrared bands on the time-scales probed.

4.6 Swope Telescope

An optical image of the FRB field was taken 16 h 51 m after the burst event with the 1-m Swope Telescope at Las Campanas. The field was re-imaged with the Swope Telescope on May 17, 2 d after the FRB. No variable optical sources were identified in the observations FOV, 1.92 deg^2, to a limiting magnitude of $R = 16$.

4.7 Palomar Transient Factory

The intermediate Palomar Transient Factory (iPTF) uses the 1.2-m Samuel Oschin Telescope at Palomar Observatory at *R* band with 60 s exposure times to search for optical transients over 8.1 deg^2 (Law et al. 2009; Rau et al. 2009). The iPTF was triggered within 12 h and observations began approximately 18 h after FRB 140514 on the night of May 15. Four epochs of suitable data were taken of the field on May 15, 16, 17, and 19 with an *R*-band limiting magnitude of 19.1, 19.3, 19.3, and 19.1, respectively. All data were reduced using the IPAC pipeline (Laher et al. 2014) with photometric calibration described in Ofek et al. (2012). Several stars and asteroids were identified in the field over the four epochs; however, no variable or fading candidates were identified that might be associated with FRB 140514.

4.8 Magellan Telescope

Deep images of the FRB field were taken with the 6.5-m Baade telescope at Las Campanas in the *R* and *I* bands on May 17, 3 d after FRB 140514, and again on July 8, 55 d later. These data have provided the deepest optical images of the field, with a limiting magnitude, R, $I = 22.5$ in the first epoch and R, $I = 24.5$ in the

second epoch with a FOV of 635 arcmin^2. The first observation was seven 2-min exposures and the second consisted of five 5-min exposures. These observations identified one extended object in the field that appeared with a magnitude of $R = 21.9 \pm 0.1$ in the first epoch and was not detected in the second observation through point source searches. Due to its extended nature in the observation this source has been identified as a moving object such as a satellite or debris passing through the field and was not flagged as a potentially associated candidate.

4.9 SkyMapper

A ToO was sent to the 1.35-m SkyMapper telescope at Siding Spring in Australia. Observations were taken on the night of the May 16, 2 d after FRB 140514, and May 23, 9 d after the event. The SkyMapper FOV is 5.7 deg^2 and both images were centred on the FRB coordinates using the Hα filter which was in place for those nights. No variable objects were seen across the two epochs of data through difference imaging.

4.10 Effelsberg Radio Telescope

The field was observed at 1.4 GHz (21 cm), 2.7 GHz (11 cm), and 4.85 GHz (6 cm) using the 100-m Effelsberg Radio Telescope in Germany five days after FRB 140514. A single object was detected in the field with $S_{1.4\,\mathrm{GHz}} = 447 \pm 30$ mJy and a spectral index of $\alpha = -0.54 \pm 0.08$. A source at this position was also visible in the NVSS with $S = 493 \pm 15$ mJy, which is consistent, indicating no change in brightness after FRB 140514.

4.11 Keck spectroscopy

Spectroscopic follow-up of XRT1, XRT2, and GMRT1 was performed on May 27, 13 d after FRB 140514, using the Low Resolution Imaging Spectrometer on the 10-m Keck I telescope (Oke et al. 1995). Based on their spectral properties, XRT1 and XRT2 were identified as AGN, and GMRT1 was identified as a starburst galaxy with a high star formation rate. The spectral features of GMRT1 were typical of a starburst galaxy and there were no strong or unexpected spectral line features that might hint at unusual activity.

4.12 Nordic Optical Telescope spectroscopy

Additional spectroscopic observations were performed using the 2.5-m Nordic Optical Telescope (NOT) at La Palma for XRT1 and XRT2, 2.4 and 21.4 d after FRB 140514, respectively. Both were confirmed to be AGN. The brighter X-ray source, XRT1, is a Seyfert type 1.9 galaxy at $z = 0.195$, and the XRT2 is an AGN with $z = 0.51$. The spectra of both sources were not observed to evolve between the two observations with NOT and Keck.

5 INTERPRETATION AND DISCUSSION

Over the various epochs and wavelengths detailed in Section 4, no afterglow-like variable counterparts were detected that could be identified as a candidate host or progenitor associated with the radio observation of FRB 140514. Here, we consider the possible sources and mechanisms that might produce the observed behaviour and set limits on FRB detectability at other wavelengths on hour-to-day time-scales.

5.1 Polarization

Any progenitor theory of FRBs must explain the observed polarization; several possibilities exist for this FRB. We consider three here.

(i) *Case 1*: the emission is intrinsically only circularly polarized, as observed, perhaps also with low linear polarization.
(ii) *Case 2*: the emission is intrinsically linearly and circularly polarized, but the linear polarization was undetectable due to bandwidth depolarization by severe Faraday rotation.
(iii) *Case 3*: The emission is intrinsically unpolarized and circular polarization (CP) is scintillation induced.

Case 1. Few sources observed at radio frequencies produce only circularly polarized emission. The flare star AD Leonis has been observed to produce 90–100 per cent circularly polarized radio emission coincident with optical flares (Osten & Bastian 2006, 2008); the brown dwarf TVLM 513−46546 and the Sun have also been observed to emit 100 per cent circularly polarized bursts at GHz frequencies, both attributed to cyclotron maser emission (Melrose & Dulk 1982; Hallinan et al. 2007). These radio bursts typically last seconds to minutes with no frequency-dependent time delays comparable to the ν^{-2} dispersive sweep seen for FRBs. The level of CP in FRB 140514 ($\sim$21 per cent) is also much lower than that observed in other cases. Some AGN have been observed with more CP than linear (Homan & Lister 2006); however, the overall levels of CP were much lower (typically $\geq$0.3 per cent) and would not have been detected here. Some single pulses from pulsars have been observed with high fractional circular polarization and a small linear component and this FRB may represent such a state (Levin et al. 2012; Osłowski et al. 2014).

Case 2. The maximum RM for the search in Section 3 describes the complete depolarization of a 100 per cent linearly polarized source. A weaker level of linear polarization might have been depolarized at these frequencies by RMs of the order of $\sim 10^4$ rad m^{-2} and greater, however such values are still several orders of magnitude greater than theorized for Faraday rotation in the IGM (Akahori & Ryu 2010). Additionally, if the source originated at some redshift and the emission observed at 1.4 GHz was redshifted into our observing band, the Faraday rotation at the source would need to be much higher given the frequency of emission. The electron density component of the RM is constrained by the source DM, thus high magnetic fields are required to produce the necessary rotation of the plane of linear polarization. Such high rotation measures are incredibly rare, but have been observed in the magnetar PSR J1745-2900 near the Galactic Centre (Eatough et al. 2013; Shannon & Johnston 2013). The required path-averaged magnetic field to produce these rotation measures would be $\geq$250 μG for FRB 140514. A source located within 1 pc of the centre of its host galaxy, with the host contributing 100 pc cm^{-3} to the total DM, could produce path-averaged magnetic field strengths of 10–100 μG. FRB 140514 would need to have originated in a region of similar magnetic field strength to produce the necessary Faraday rotation. It is also worth noting that observations of a radio-loud magnetar have shown the occurrence of an infrequent state in which the emission is highly circularly polarized with a lower-than-average linear component (Levin et al. 2012). With a sufficiently strong integrated magnetic field along the line of sight, the linear component could be completely depolarized for a magnetar flare. Such a flare would still be in good agreement with the models and conditions put forward in Kulkarni et al. (2014).

Case 3. It has been theorized that scintillation-induced CP may arise in an intrinsically unpolarized source (Macquart & Melrose

2000). In the diffractive regime – for pulsars and other Galactic sources – CP up to ∼15 per cent may be induced by a birefringent medium at low frequencies, and in the refractive regime ∼0.1 per cent may be induced for extragalactic sources observed at higher radio frequencies. Such scintillation requires the presence of an RM gradient across the turbulent region, which we cannot constrain with available data. The ∼15 per cent CP in the Macquart & Melrose (2000) simulation was derived from the Vela pulsar, an extreme example within the pulsar population, being bright, young, and surrounded by a turbulent and high-velocity medium (Hamilton, Hall & Costa 1985; Petroff et al. 2013). Such an object would very likely be detected in future follow-up of the detection position.

Of the three possibilities presented here, *Case 3* requires very specialized Galactic conditions to produce CP close to the level observed in this work and is not the best model to describe the observed FRB CP. Both *Case 1* and *Case 2* require CP intrinsic to the source, and vary only in on the predicted level of linear polarization.

Recent theoretical work has speculated that mechanisms to produce sufficiently high brightness temperatures for observed FRBs require beaming of coherent emission (Katz 2014) which would produce intrinsic linear polarization, making *Case 2* more appealing. The required brightness temperature $T_{\rm B}$ for FRB 140514, ignoring relativistic effects, can be calculated using

$$T_{\rm B} \simeq 10^{36}{\rm K} \left(\frac{S_{\rm peak}}{\rm Jy}\right) \left(\frac{\rm GHz}{\nu}\right)^2 \left(\frac{\rm ms}{\Delta t}\right)^2 \left(\frac{d}{\rm Gpc}\right)^2 \frac{(1+z)^4}{\gamma^2}, \quad (4)$$

where $S_{\rm peak}$ is the flux density, ν is the centre observing frequency, Δt is the pulse width, and d is the comoving distance (Lorimer & Kramer 2004). For FRB 140514, we estimate a brightness temperature $T_{\rm B} = 5.3 \times 10^{35}$ K, not including relativistic effects. Such a high brightness temperature is beyond the regime of pulses from typical pulsars but approaches what is seen in the brightest nanoshot pulses from the Crab pulsar (10^{41} K) (Hankins & Eilek 2007). Temperatures in this regime preclude synchrotron emission, thus making it likely that the pulse emission is coherent (Readhead 1994). However, no linear polarization was detected, an unexpected result given previous observations of coherent emission mechanisms at such high brightness temperatures (Hankins et al. 2003).

An additional theory of FRB origins put forward by Mottez & Zarka (2014) suggests that FRBs are created in the Alfvén wings of a planet orbiting a neutron star within the pulsar wind via the electron cyclotron maser (ECM) instability at Gpc distances. This theory predicts strong CP such as the 100 per cent circular emission seen in other objects that emit via ECM such as the M dwarves observed by Hallinan et al. (2008). While this is the only current theory that explicitly predicts circularly polarized emission from FRBs, a significant fraction of the intrinsic circular polarization (>50 per cent) would have been lost by some unknown mechanism for FRB 140514 to explain the observed polarized profile.

We then conclude that *Case 1* or *Case 2* may be the best explanation of the observed polarization for FRB 140514, although, the non-detection of linear polarization at 1.4 GHz might require extremely high magnetic fields to produce the necessary Faraday rotation, possibly near a Galactic Centre.

In the future, more sensitive measurements of FRB polarization may be possible with coherent baseband capture buffers such as the CASPER Parkes Swinburne Recorder installed on the centre beam of the multibeam receiver at Parkes, and those being designed for the Square Kilometre Array.

5.2 Possible connection with FRB 110220

FRB 140514 was discovered in radio follow-up observations of a previous FRB event, FRB 110220, published in Thornton et al. (2013). FRB 110220 was the most extensively analysed FRB in this sample as it was the brightest, detected with an S/N of 49, an extremely high DM of 944 cm^{-3} pc, a $\nu^{-2.003 \pm 0.006}$ dispersion relation, and a significant scattering tail.

FRB 140514 was discovered in a grid pointing around the position of FRB 110220: the centre beam of the receiver was centred 9 arcmin away from the detection beam position for FRB 110220. Given the overlap of the 14 arcmin beam on-sky between the two FRBs it is tempting to make an association. A few considerations must be made before attributing both events to the same source – the probability of detecting a new source given the FRB rate and the time on-sky for these observations, the physical mechanism necessary to produce a large change in DM over the time between detections, and the time of day and position of the telescope at the time of each detection.

The probability of detecting a new FRB in our observations can be calculated using the formula

$$P(N|M) = \alpha^N (1+\alpha)^{-(1+M+N)} \frac{(M+N)!}{M!\,N!}, \quad (5)$$

derived in Petroff et al. (2014) to find the likelihood of detecting N FRBs in our survey based on M detections in a previous survey with a ratio between their cumulative time on-sky of α. This FRB campaign (with extra time granted by the scheduler) has spent 85 h on-sky over the duration of the survey. The probability of finding a new FRB in these data, given the FRB rate from Thornton et al. (2013) is ∼32 per cent, if FRBs are non-repeating.

Recent results from Burke-Spolaor & Bannister (2014) and Petroff et al. (2014) have both addressed the possibility of a lower rate based on results from searches at lower Galactic latitudes, possibly due to foreground effects. Using the rate derived in Burke-Spolaor & Bannister (2014), we estimate a much lower detection probability of ∼2 per cent from our survey. However, Burke-Spolaor & Bannister (2014) note that the number of detectable FRBs may be heavily latitude dependent, with different rates applying for surveys at high and low Galactic latitude. In the absence of an expression for this dependence, we will continue to use the probability derived from the results of Thornton et al. (2013) as their survey explicitly sampled the region around FRB 140514. Based on comparison with previous rate estimates it is therefore not unexpected that we would find a new FRB in this project.

FRB 110220 was observed with a DM of 944.7 cm^{-3} pc, compared to a DM of 562 cm^{-3} pc for FRB 140514, a difference of 380 cm^{-3} pc for events separated by 1179 d. This is a temporal variation in the DM which is four orders of magnitude greater than what is seen for pulsars in the most turbulent environments (e.g. $|{\rm dDM/d}t| = 0.18 \pm 1$ cm^{-3} pc yr^{-1} for PSR J1833-0827; Petroff et al. 2013).

In order for such large DM variations to be observed for these two FRBs, most of the dispersive medium for FRB 110220 would be local to the source and thus extremely dense. Dennison (2014) and Tuntsov (2014) have both argued that if the majority of the DM were produced in a dense plasma around the emission region, such as in a stellar corona, the observed dispersion relation would be poorly fit by a ν^{-2} relation, which would have been easily detected in the analysis conducted by Thornton et al. (2013) for FRB 110220 and the analysis conducted here for FRB 140514. Additionally, FRB 140514 was discovered at 03:14 AEST local time at a telescope orientation in azimuth and elevation of (84.°9, 30.°3) while FRB

110220 occurred at 11:52 AEST local time at a telescope orientation of (29°.9, 66°.3).

We conclude that FRB 110220 and FRB 140514 are different sources, and their proximity is purely due to sampling bias in our choice of observing location. This proximity does not affect the proposed cosmological origin of FRBs.

5.3 Limits on a varying counterpart

In explosions such as supernovae (SNe) and superluminous supernovae (SLSNe), or in long gamma-ray bursts (GRBs), a counterpart is detectable as an object of varying brightness in subsequent observations. Variations in brightness would be observable on time-scales of hours (for a long GRB), days (for typical SNe) or weeks (for a SLSN). Such variations were not seen in our data in X-ray, NIR, optical, or radio regimes. Additionally, no gamma-ray emission from the field was observed by the interplanetary network in either the hard or soft gamma-ray energy bands, ruling out all but soft, short GRBs (Pal'shin, private communication). Therefore, no variable counterpart or related transient emission was observed in association with FRB 140514. From the extensive data set collected in this analysis, we can then place limits on the magnitude of any potential afterglow for FRB 140514.

We place the limits on related transient emission at 20.0 in *J* band (1.65 μm), 19.2 in *H* band (1.2 μm), 18.6 in *K* band (2.2 μm), 24.5 in *R* band, 24.5 in *I* band, 1.5 mJy at 4.8 GHz, 60 mJy at 1–3 GHz, and 125 μJy at 610 MHz. We compare these limits to light curves of known variable SNe and GRBs (Fig. 3) and find that many nearby sources would have been detected in this analysis (Galama et al. 1998; Kulkarni et al. 1998; Evans et al. 2007; Rest et al. 2011). We rule out local SLSNe and nearby ($z < 0.3$) Type Ia SNe, as well as slow transients with variations greater than 2 mag AB between our epochs of observation. We also rule out an FRB association with long GRBs.

Such constraints make associations between FRB 140514 and some SNe or long GRBs highly unlikely. Any theoretical description of FRB emission must adhere to these constraints.

5.4 Host galaxies

Given the large error radius of the Parkes beam (7.2 arcmin) an identification of a host galaxy in the original radio detection was not possible and no other association was detected at other wavelengths as no variable sources were identified in the field. In our follow-up observations, three sources of interest were detected in the field of FRB 140514 by *Swift* and the GMRT: two X-ray luminous AGN and one radio-loud starburst galaxy. The identification of AGN within a 15 arcmin beam is not unexpected; approximately three AGN are expected to occur within the area of the Parkes beam out to $z = 2$ based on cosmological distribution alone (Fiore et al. 2003). Finding a starburst galaxy in our field is also likely based on galaxy distribution studies (Hirashita et al. 1999). Therefore, we are unable to make any robust connection between the FRB and any other objects identified in the field on probability arguments alone.

6 CONCLUSIONS

We report here on an FRB discovered in real-time at 1.4 GHz at the Parkes radio telescope. FRB 140514 was the first real-time FRB detection and the first with polarization information. The pulse was observed to be 21 ± 7 per cent (3σ) circularly polarized with a 1σ upper limit of 10 per cent on linear polarization which was not detected. We coordinated the fastest and largest follow-up effort ever undertaken for an FRB, with data from 12 telescopes. No associated slow transient, progenitor, or host galaxy was identified,

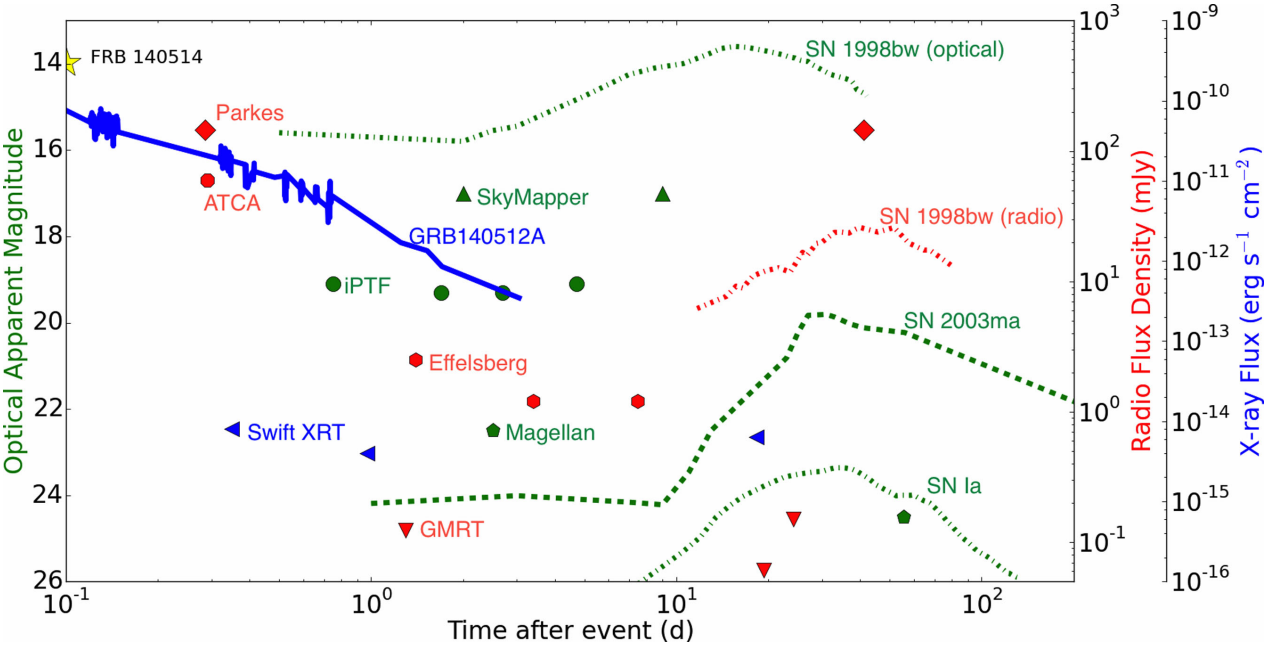

Figure 3. The limits for optical in apparent magnitude (green), radio flux density in mJy (red), and X-ray flux in erg cm^{-2} s^{-1} (blue) of our observations of the field of FRB 140514 from eight telescopes that fully sampled the Parkes beam. Colours of data points refer to the axis scale of the same colour. Light curves from GRB140512A ($z = 0.725$), 1.4 GHz radio data and *R*-band optical data for supernova SN1998bw ($z \sim 0.008$), *R*-band data for SLSN SN2003ma ($z = 0.289$) and an *R*-band light curve for a typical Type Ia SN ($z = 0.5$) have been included for reference (Galama et al. 1998; Evans et al. 2007; Rest et al. 2011; Kulkarni et al. 2014).

effectively ruling out any association between this FRB and an SN at $z < 0.3$ or long GRB. A tighter constraint on FRB origins in the future will require not only robust and immediate triggering or commensal observing at multiple observatories, but also improved sky localization of radio pulses within FRB and pulsar surveys. We note that any theory of FRB origin must satisfy the polarization, brightness temperature, and afterglow limits put forward in this analysis.

PUBLIC DATA RELEASE

The data presented in this paper are made available through Research Data Australia[4] and can be processed using the publicly available HEIMDALL single pulse processing software and the PSRCHIVE software package.

ACKNOWLEDGEMENTS

The Parkes radio telescope and the ATCA are part of the Australia Telescope National Facility which is funded by the Commonwealth of Australia for operation as a National Facility managed by CSIRO. Parts of this research were conducted by the Australian Research Council Centre of Excellence for All-sky Astrophysics (CAASTRO), through project number CE110001020. We thank the staff of the GMRT that made these observations possible. GMRT is run by the National Centre for Radio Astrophysics of the Tata Institute of Fundamental Research. Research with the ANU SkyMapper telescope is supported in part through ARC Discovery Grant DP120101237. We thank the Carnegie Supernova Project team (PI M. Phillips) and intermediate Palomar Transient Factory team (PI S. Kulkarni) for promptly taking follow-up data. Part of the funding for GROND (both hardware as well as personnel) was generously granted from the Leibniz-Prize to Professor G. Hasinger (DFG grand HA 1850/28-1). The Dark Cosmology Centre is supported by the Danish National Research council. We thank A. Krauss for prompt observations with the Effelsberg Radio Telescope. Partly based on observations made with the NOT, operated by the Nordic Optical Telescope Scientific Association at the Observatorio del Roque de los Muchachos, La Palma, Spain, of the Instituto de Astrofísica de Canarias.

We thank the anonymous referee for valuable input which improved the clarity of this paper. EP would like to thank M. Murphy, J. Cooke, and C. Vale for useful discussion and valuable comments. NDRB is supported by a Curtin Research Fellowship. CD acknowledges support through EXTraS, funded from the European Union's Seventh Framework Programme for research, technological development and demonstration under grant agreement no 607452. MMK acknowledges generous support from the Hubble Fellowship and Carnegie-Princeton Fellowship. DM acknowledged the Instrument Center for Danish Astrophysics (IDA) for support. EOO is incumbent of the Arye Dissentshik career development chair and is grateful to support by grants from the Willner Family Leadership Institute Ilan Gluzman (Secaucus NJ), Israeli Ministry of Science, Israel Science Foundation, Minerva, Weizmann-UK and the I-CORE Program of the Planning and Budgeting Committee and The Israel Science Foundation. Support for DAP was provided by NASA through Hubble Fellowship grant HST-HF-51296.01-A awarded by the Space Telescope Science Institute, which is operated by the Association of Universities for Research in Astronomy, Inc., for NASA, under contract NAS 5-26555. BPS, CW, and PT acknowledge funding from the ARC via CAASTRO and grand LF0992131.

[4] https://researchdata.ands.org.au/fast-radio-burst-frb-140514/468269

REFERENCES

Akahori T., Ryu D., 2010, ApJ, 723, 476
Burke-Spolaor S., Bannister K. W., 2014, ApJ, 792, 19
Condon J. J., Cotton W. D., Greisen E. W., Yin Q. F., Perley R. A., Taylor G. B., Broderick J. J., 1998, AJ, 115, 1693
Cordes J. M., Lazio T. J. W., 2002, preprint (astro-ph/0207156)
Deng W., Zhang B., 2014, ApJ, 783, L35
Dennison B., 2014, MNRAS, 443, L11
Eatough R. P. et al., 2013, Nature, 501, 391
Evans P. A. et al., 2007, A&A, 469, 379
Fiore F. et al., 2003, A&A, 409, 79
Galama T. J. et al., 1998, Nature, 395, 670
Gao H., Li Z., Zhang B., 2014, ApJ, 788, 189
Gehrels N. et al., 2004, ApJ, 611, 1005
Greiner J. et al., 2008, PASP, 120, 405
Hallinan G. et al., 2007, ApJ, 663, L25
Hallinan G., Antonova A., Doyle J. G., Bourke S., Lane C., Golden A., 2008, ApJ, 684, 644
Hamilton P. A., Hall P. J., Costa M. E., 1985, MNRAS, 214, 5P
Hankins T. H., Eilek J. A., 2007, ApJ, 670, 693
Hankins T. H., Kern J. S., Weatherall J. C., Eilek J. A., 2003, Nature, 422, 141
Hirashita H., Takeuchi T. T., Shibai H., Ohta K., 1999, PASJ, 51, 81
Homan D. C., Lister M. L., 2006, ApJ, 131, 1262
Hotan A. W., van Straten W., Manchester R. N., 2004, Publ. Astron. Soc. Aust., 21, 302
Ioka K., 2003, ApJ, 598, L79
Katz J. I., 2014, Phys. Rev. D, 89, 103009
Keith M. J. et al., 2010, MNRAS, 409, 619
Kulkarni S. R. et al., 1998, Nature, 395, 663
Kulkarni S. R., Ofek E. O., Neill J. D., Zheng Z., Juric M., 2014, preprint (arXiv:1402.4766)
Laher R. R. et al., 2014, PASP, 126, 674
Law N. M. et al., 2009, PASP, 121, 1395
Levin L. et al., 2012, MNRAS, 422, 2489
Loeb A., Shvartzvald Y., Maoz D., 2014, MNRAS, 439, L46
Lorimer D. R., Kramer M., 2004, Handbook of Pulsar Astronomy, Vol. 4, Cambridge Univ. Press, Cambridge
Lorimer D. R., Bailes M., McLaughlin M. A., Narkevic D. J., Crawford F., 2007, Science, 318, 777
Lyubarsky Y., 2014, MNRAS, 442, L9
Macquart J.-P., Melrose D. B., 2000, ApJ, 545, 798
Manchester R. N., Hobbs G. B., Teoh A., Hobbs M., 2005, AJ, 129, 1993
Melrose D. B., Dulk G. A., 1982, ApJ, 259, 844
Monet D. G. et al., 2003, AJ, 125, 984
Morris D. J. et al., 2002, MNRAS, 335, 275
Mottez F., Zarka P., 2014, A&A, 569, A86
Ofek E. O. et al., 2012, PASP, 124, 62
Oke J. B. et al., 1995, PASP, 107, 375
Osłowski S., van Straten W., Bailes M., Jameson A., Hobbs G., 2014, MNRAS, 441, 3148
Osten R. A., Bastian T. S., 2006, ApJ, 637, 1016
Osten R. A., Bastian T. S., 2008, ApJ, 674, 1078
Petroff E., Keith M. J., Johnston S., van Straten W., Shannon R. M., 2013, MNRAS, 435, 1610
Petroff E. et al., 2014, ApJ, 789, L26
Rau A. et al., 2009, PASP, 121, 1334
Readhead A. C. S., 1994, ApJ, 426, 51
Rest A. et al., 2011, ApJ, 729, 88
Shannon R. M., Johnston S., 2013, MNRAS, 435, L29
Spitler L. G. et al., 2014, ApJ, 790, 101
Staveley-Smith L. et al., 1996, Publ. Astron. Soc. Aust., 13, 243

Thornton D. et al., 2013, Science, 341, 53
Tuntsov A. V., 2014, MNRAS, 441, L26
Wright E. L., 2006, PASP, 118, 1711

[1]*Centre for Astrophysics and Supercomputing, Swinburne University of Technology, PO Box 218, Hawthorn, VIC 3122, Australia*
[2]*CSIRO Astronomy & Space Science, Australia Telescope National Facility, PO Box 76, Epping, NSW 1710, Australia*
[3]*ARC Centre of Excellence for All-sky Astrophysics (CAASTRO)*
[4]*Harvard–Smithsonian Center for Astrophysics, 60 Garden Street, Cambridge, MA 02138, USA*
[5]*International Centre for Radio Astronomy Research, Curtin University, Bentley, WA 6102, Australia*
[6]*Research School of Astronomy and Astrophysics, Australian National University, ACT 2611, Australia*
[7]*Cahill Center for Astrophysics, California Institute of Technology, 1200 E California Blvd, Pasadena, CA 91125, USA*
[8]*Max Planck Institut für Radioastronomie, Auf dem Hügel 69, D-53121 Bonn, Germany*
[9]*National Centre for Radio Astrophysics, Tata Institute of Fundamental Research, Pune University Campus, Ganeshkhind, Pune 411 007, India*
[10]*Max-Planck-Institut für extraterrestrische Physik, Giessenbachstrasse 1, D-85748 Garching, Germany*
[11]*Astrophysics Science Division, NASA Goddard Space Flight Center, Greenbelt, MD 20771, USA*
[12]*Observatories of the Carnegie Institution for Science, 813 Santa Barbara Street, Pasadena, CA 91101, USA*
[13]*Jet Propulsion Laboratory, California Institute of Technology, 4800 Oak Grove Drive, Pasadena, CA 91104, USA*
[14]*Jodrell Bank Centre for Astrophysics, University of Manchester, Alan Turing Building, Oxford Road, Manchester M13 9PL, UK*
[15]*Dark Cosmology Centre (DARK), Niels Bohr Institute, University of Copenhagen, Juliane Maries Vej 30, DK-2100 Copenhagen Ø, Denmark*
[16]*Department of Particle Physics & Astrophysics, Weizmann Institute of Science, Rehovot 76100, Israel*
[17]*INAF - Osservatorio Astronomico di Cagliari, Via della Scienza 5, I-09047 Selargius (CA), Italy*
[18]*Kavli Institute for Astronomy and Astrophysics, Peking University, Beijing 100871, China*
[19]*Institut d'Astrophysique de Paris, Sorbonne Universités, UPMC Univ Paris 06, UMR 7095, F-75005 Paris, France*
[20]*CNRS, UMR 7095, Institut d'Astrophysique de Paris, 98 bis Boulevard Arago, F-75014 Paris, France*

This paper has been typeset from a TEX/LATEX file prepared by the author.